Anal. Chem. **2010,** *82,* 10015–10020

Flow-Through vs Flow-Over: Analysis of Transport and Binding in Nanohole Array Plasmonic Biosensors

Carlos Escobedo,[†] Alexandre G. Brolo,[‡] Reuven Gordon,[§] and David Sinton*,[†]

Mechanical Engineering, Chemistry, and Electrical and Computer Engineering, University of Victoria, Victoria, BC, Canada

We quantify the efficacy of flow-through nanohole sensing, as compared to the established flow-over format, through scaling analysis and numerical simulation. Nanohole arrays represent a growing niche within surface plasmon resonance-based sensing methods, and employing the nanoholes as nanochannels can enhance transport and analytical response. The additional benefit offered by flow-through operation is, however, a complex function of operating parameters and application-specific binding chemistry. Compared here are flow-over sensors and flow-through nanohole array sensors with equivalent sensing area, where the nanohole array sensing area is taken as the inner-walls of the nanoholes. The footprints of the sensors are similar (e.g., a square 20 μm wide flow-over sensor has an equivalent sensing area as a square 30 μm wide array of 300 nm diameter nanoholes with 450 nm periodicity in a 100 nm thick gold film). Considering transport alone, an analysis here shows that given equivalent sensing area and flow rate the flow-through nanohole format enables greatly increased flux of analytes to the sensing surface (e.g., 40-fold for the case of $Q = 10$ nL/min). Including both transport and binding kinetics, a computational model, validated by experimental data, provides guidelines for performance as a function of binding time constant, analyte diffusivity, and running parameters. For common binding kinetics and analytes, flow-through nanohole arrays offer ~10-fold improvement in response time, with a maximum of 20-fold improvement for small biomolecules with rapid kinetics.

Metallic films with ordered arrays of nanoholes exhibit surface plasmon resonance (SPR) that facilitates enhanced optical transmission through the holes.[1−4] The influence of the near-surface refractive index on the resulting transmission has been employed for sensing applications.[5,6] Nanohole arrays represent a growing niche within SPR-based sensing methods.[7] Specifically, as compared to traditional SPR sensing, nanohole arrays can provide a smaller foot-print, denser integration, increased potential for multiplexing and simplified collinear optical detection in which analyte binding is determined directly from light that is transmitted through the holes.[7−10] Moreover, the sensitivity of nanohole arrays has been reported to be similar to traditional SPR.[11] Ferreira et al.[6] demonstrated that in contrast to traditional SPR, the top gold surface is not necessarily the dominant sensing surface in nanohole arrays. Rather, the molecular binding that occurs on the inner surface of the nanoholes can dominate the sensor response.[6] This finding highlighted the importance of transporting analytes to the interior of nanoholes.

In order to enhance the transport of analyte to the in-hole sensing surface we developed a flow-through nanohole array sensing format.[12] All previous nanohole array sensing involved dead-ended holes and thus relied on cross-stream analyte transport within a microchannel flow as is typical for surface based biosensors. This traditional flow-over format is shown schematically in Figure 1a. In contrast, the flow-through strategy capitalizes on the unique nature of nanohole plasmonic sensing elements in that they are also fundamentally nanochannels.[12] The flow-through strategy is shown in Figure 1b. An array of through-nanoholes serves as nanochannels in parallel and provides an analyte sieving action that is unique among surface-based sensors. Our experimental results demonstrated proof-of-concept flow-through biosensing and a 6-fold improvement in response time compared to the traditional microfluidic flow-over method when applied to monitor a monolayer adsorption process.[12] More recently, Yanik

* To whom correspondence should be addressed. E-mail: dsinton@uvic.ca.
† Mechanical Engineering.
‡ Chemistry.
§ Electrical and Computer Engineering.

(1) Ebbesen, T. W.; Lezec, H. J.; Ghaemi, H. F.; Thio, T.; Wolff, P. A. *Nature* **1998**, *391*, 667–669.
(2) Genet, C.; Ebbesen, T. W. *Nature* **2007**, *445*, 39–46.
(3) Barnes, W. L.; Dereux, A.; Ebbesen, T. W. *Nature* **2003**, *424*, 824–830.
(4) Kwak, E. S.; Henzie, J.; Chang, S. H.; Gray, S. K.; Schatz, G. C.; Odom, T. W. *Nano Lett.* **2005**, *5*, 1963–1967.
(5) Gordon, R.; Sinton, D.; Kavanagh, K. L.; Brolo, A. G. *Acc. Chem. Res.* **2008**, *41*, 1049–1057.
(6) Ferreira, J.; Santos, M, J. L.; Rahman, M. M.; Brolo, A. G.; Gordon, R.; Sinton, D.; Girotto, E. M. *J. Am. Chem. Soc.* **2009**, *131*, 436+.
(7) Sinton, D.; Gordon, R.; Brolo, A. G. *Microfluid. Nanofluid.* **2008**, *4*, 107–116.
(8) DeLeebeeck, A.; Kumar, L. K. S.; deLange, V.; Sinton, D.; Gordon, R.; Brolo, A. G. *Anal. Chem.* **2007**, *79*, 4094–4100.
(9) Brolo, A. G.; Gordon, R.; Leathem, B.; Kavanagh, K. L. *Langmuir* **2004**, *20*, 4813–4815.
(10) Lindquist, N. C.; Lesuffleur, A.; Im, H.; Oh, S. H. *Lab Chip* **2009**, *9*, 382–387.
(11) Tetz, K. A.; Pang, L.; Fainman, Y. *Opt. Lett.* **2006**, *31*, 1528–1530.
(12) Eftekhari, F.; Escobedo, C.; Ferreira, J.; Duan, X.; Girotto, E. M.; Brolo, A. G.; Gordon, R.; Sinton, D. *Anal. Chem.* **2009**, *81*, 4308–4311.

10.1021/ac101654f © 2010 American Chemical Society
Published on Web 11/16/2010

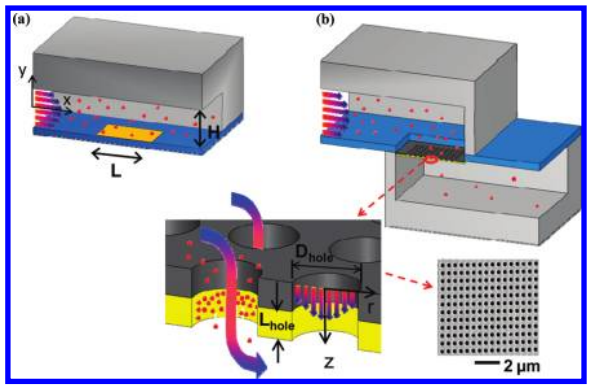

Figure 1. Schematic representation of the two sensing formats considered in this work: (a) a typical flow-over format with a square surface-based sensor within a microfluidic channel, and (b) the flow-through nanohole array format where analyte solution passes from one microchannel to another via an array of nanoholes/nanochannels in parallel.

et al.[13] demonstrated a 14-fold improvement in the mass transport rate of IPA as compared to an otherwise similar flow-over system, and Jonsson et al.[14] presented flow-through plasmonic sensing using a short-range ordered nanoscale pores. These recent isolated results indicate the excitement and promise surrounding flow-through nanohole based plasmonic sensing. Facilitating flow-through sensing is, however, more complicated than flow-over which can be achieved with a single fluidic channel. For a given application the potential benefit offered by flow-through sensing will be a function of operating parameters and binding kinetics of the specific analyte system.

Transport and binding kinetics have been studied extensively for the flow-over format typical of surface based microsensors and nanowires.[15−23] Zimmermann et al.[24] investigated the analyte surface capture using a 2-D model under different input parameters such as flow rate and binding kinetics constants. Hu et al.[17] presented a 2-D flow-over model and demonstrated better performance with electrokinetically driven immunoassays over pressure-driven ones in terms of reaction kinetics. Fu et al.[18] presented a 2-D computational model to identify operating ranges for sensitivity improvement in microfluidic heterogeneous immunoassays. Squires et al.[21] provided an elegant and practical analysis of microfluidic and nanowire surface-based sensors highlighting limiting factors in each case.

The parallel nature and length scales involved in the flow-through sensing is a deviation from the established flow-over format. Recent experimental demonstrations show significant improvements in response for isolated monolayer adsorption and analyte systems.[12−14,17,25,26] The efficacy of this strategy as compared to the established flow-over method has not, however, been quantified as a function of running parameters and binding kinetics, and no guidelines are available to assess applicability as a function of surface chemistry specifics.

In this work, the efficacy of flow-through nanohole sensing, as compared to the established flow-over format, is quantified as a function of operating parameters and surface chemistry through scaling analysis and numerical simulation. Flow-through and flow-over sensors are compared with equivalent sensing area. That is, the planar sensing area of the flow-over sensor is equivalent to the total inner-wall area of the nanoholes in the nanohole array. The footprints of the sensors are similar (e.g., a square 20 μm wide flow-over sensor has an equivalent sensing area as a square 30 μm wide array of 300 nm diameter nanoholes with 450 nm periodicity in a 100 nm thick gold film). The goals of this work are to (1) quantify the advantage offered by flow-through sensing; and (2) serve as a guide to assess the benefit of employing a flow-through scheme for a given sensing application.

BACKGROUND

Model Systems. The two sensing formats considered in this work are shown schematically in Figure 1. A typical flow-over format with a square surface-based sensor within a microfluidic channel is shown in Figure 1a, and the flow-through nanohole array format is shown in Figure 1b. For simplicity, the flow-over sensor geometry was fixed as square with a side length equivalent to the channel width, L, in a microchannel of height, H. The flow-through sensor assumed an array of parallel nanoholes milled through a 100 nm thick silicon nitride membrane with a 100 nm gold coating. The size of the flow-through sensor array was set such that the total inner-wall sensing area was equivalent to the area of the flow-over sensor. In both cases, the analyte was transported by a pressure-driven flow.

Simulations. Fluid flow and mass transport were modeled in both systems using Finite Element Analysis software COMSOL Multiphysics (COMSOL, Sweden) under the assumption of unidirectional 2-D pressure-driven flow, and employing the Stokes flow approximation typical of microfluidic and nanofluidic liquid flows.[27] The flow-over sensor model included a 2D Cartesian domain along the midplane of the microchannel as shown in Figure 1a. The flow-through nanohole array based sensor model is a 2-D axisymmetric domain along a nanohole cross section, as shown in Figure 1b. Details on the computational models used for the simulations can be found in the Supporting Information (SI). In order to validate the computational model, modeling results were compared with experimental results for the flow-through geometry. With respect to characteristic binding response time, the model and the experimental data agreed to within ±5%. Details on the model validation and the computational and experimental results are provided in the SI.

(13) Yanik, A. A.; Huang, M.; Artar, A.; Chang, T. Y.; Altug, H. *Appl. Phys. Lett.* **2010**, *96*.
(14) Jonsson, M. P.; Dahlin, A. B.; Feuz, L.; Petronis, S.; Hook, F. *Anal. Chem.* **2010**, *82*, 2087–2094.
(15) Sheehan, P. E.; Whitman, L. J. *Nano Lett.* **2005**, *5*, 803–807.
(16) Squires, T. M.; Quake, S. R. *Rev. Mod. Phys.* **2005**, *77*, 977–1026.
(17) Hu, G.; Gao, Y.; Li, D. *Biosens. Bioelectron.* **2007**, *22*, 1403–1409.
(18) Fu, E.; Nelson, K. E.; Ramsey, S. A.; Foley, J. O.; Helton, K.; Yager, P. *Anal. Chem.* **2009**, *81*, 3407–3413.
(19) Lebedev, K.; Mafé, S.; Stroeve, P. *J. Colloid Interface Sci.* **2006**, *296*, 527–537.
(20) Parsa, H.; Chin, C. D.; Mongkolwisetwara, P.; Lee, B. W.; Wang, J. J.; Sia, S. K. *Lab Chip* **2008**, *8*, 2062–2070.
(21) Squires, T. M.; Messinger, R. J.; Manalis, S. R. *Nat. Biotechnol.* **2008**, *26*, 417–426.
(22) Feuz, L.; Jonsson, P.; Jonsson, M. P.; Hook, F. *ACS Nano* **2010**, *4*, 2167–2177.
(23) Kim, D. R.; Zheng, X. L. *Nano Lett.* **2008**, *8*, 3233–3237.
(24) Zimmermann, M.; Delamarche, E.; Wolf, M.; Hunziker, P. *Biomed. Microdevices* **2005**, *7*, 99–110.
(25) Anker, J. N.; Hall, W. P.; Lyandres, O.; Shah, N. C.; Zhao, J.; Van Duyne, R. P. *Nat. Mater.* **2008**, *7*, 442–453.
(26) Canpean, V.; Astilean, S. *Lab Chip* **2009**, *9*, 3574–3579.
(27) Jensen, M. J.; Stone, H. A.; Bruus, H. *Phys. Fluids* **2006**, *18*.

Quantification of Transport to the Sensing Surface. Sensing requires transport of analyte to the surface and subsequent binding. The idealized case where the binding kinetics are very rapid and the sensor does not saturate provides a useful comparison of the transport achieved with each sensor format. For this case, analyte molecules are transported to the sensing area at steady state through a combination of convection and diffusion. The total molecular flux input into the system, J_0, is a function of the bulk concentration, c_0, and the total flow rate, Q. (In this work, flux, as indicated by a capital J, corresponds to the flux density integrated over area, and is thus a scalar.) The molecular flux to the sensing surface is the diffusive flux, J_D, which scales with the sensing area, A, diffusivity, $\mathscr{D}$, bulk concentration, c_0, and scales inversely with the thickness of the concentration gradient at the surface, δ[21] (see also the analyte depletion zone discussion in the SI). The total analyte flux to the sensing surface, J_D, was quantified here through integrating the flux density at the sensor surface in the numerical simulations. While nondimensionalization of transport parameters can be insightful (an elegant treatment is provided by Squires et al.[21]), the dimensional form of the molecular flux to the sensor surface J_D, (mol/s) was employed here for clarity in comparing transport between the flow over and flow-through cases. The transport to the sensor can also be represented as a fraction of the total molecular flux into the system, or J_D/J_0.

Quantification of Binding Kinetics. The basis for the parameter employed to quantify, and generalize, binding kinetics is explained here. Considering the case of where transport of analyte to active sites occurs much more rapidly than the binding kinetics (or "perfect transport"), the rate of change of surface concentration $c_S(t)$ of analyte adsorbed at the sensing surface, assuming first-order Langmuir kinetics,[28] is described by

$$\frac{\partial c_S}{\partial t} = k_{on} c_0 (b_0 - c_S) - k_{off} c_S \quad (1)$$

where k_{on} is the adsorption constant, k_{off} is the desorption constant, c_0 is the analyte concentration in the bulk and b_0 is the total surface concentration of active potential binding sites.

Equation 1 yields an analytical expression[17,29−31] for the surface concentration of adsorbed species as follows:

$$c_S(t) = c_S^{Eq}(1 - e^{-t/\tau}),\ c_S^{Eq} = \frac{b_0 c_0 k_{on}}{k_{on} c_0 + k_{off}},$$
$$K_A = k_{on}/k_{off}, \tau = (k_{on} c_0 + k_{off})^{-1} \quad (2)$$

where c_S^{Eq} is the equilibrium surface concentration as defined by the Langmuir adsorption equation, K_A is the affinity constant, and the time scale, τ, characterizes the time required for the sensor to reach the equilibrium concentration.[21] On this basis, τ is used in this work to quantify and compare the binding kinetics of various analyte systems.

RESULTS AND DISCUSSION

The efficacy of flow-through nanohole array based sensing depends on both transport and binding kinetics. The flow-through approach has implications mainly for transport. The scaling analysis below first focuses on the role of transport in isolation, using the assumption of perfect, rapid, reaction kinetics. Physically, this situation corresponds to a sensing surface that absorbs analyte immediately and never saturates. The value in considering this simplified case is that the analyte transport can be quantified in isolation from binding/saturation considerations. Following these transport-only analyses, both transport and binding kinetics are included.

Transport Scaling Analysis. For the flow-over case (Figure 1a) with rapid surface reaction kinetics, the flux of analyte to the sensing surface is a function of Peclet number, the ratio of the total convective flux of molecules to the diffusive flux at the sensing surface. Based on channel height, H, average velocity, U_{ch}, and diffusivity, $\mathscr{D}$, the Peclet number is given by $Pe_{ch} = U_{ch}H/\mathscr{D}$.[21]

The flow-through case (Figure 1b) is a nanohole array with the same sensing area as the flow-over case, and is provided the same solution concentration at the same volume flow rate, Q. The sensing area of a nanohole array is taken as the inner hole surface,[6] and thus the number of nanoholes required for equivalent sensing area to that of a square flow-over sensor is $N = L^2/A_{active}$ where the sensing area for a nanohole of diameter, D, and gold thickness, L_{hole}, is $A_{active} = \pi D L_{hole}$. The resulting number of holes is $N = L^2/\pi D L_{hole}$. For the case of $L = 20$ μm, $L_{hole} = 100$ m and $D = 300$ nm, the number of holes is approximately 4240, which is an array with around 65 by 65 holes. With a periodicity of 450 nm, the array will extend over an area of approximately 30×30 μm. Such a configuration is typical of nanohole array based sensors.[10,32−34] It is noteworthy that for typical flow-through nanohole geometries, the total footprint of the flow-through nanohole array is on the same order of magnitude as the planar flow-over sensor of identical sensing area. The total flow rate is divided between N number of holes, resulting in an in-hole average velocity of $U_{hole} = U_{ch}(H/L)(4L_{hole}/D)$. Since the diameter of the hole and the thickness of the gold are typically similar ($L_{hole} \sim 100$ nm is thick enough to be optically opaque but thin enough to mill through using a focused ion beam[35]) the term $(4L_{hole}/D)$ is a small correction, on the order of unity. Thus for a microchannel of approximately square cross-section ($L \sim H$) the average flow velocity in the flow-over case is approximately equivalent to that inside the nanoholes. The resulting Peclet number in the nanoholes is given by,

$$Pe_{hole} = \frac{U_{hole} D}{\mathscr{D}} = \frac{4 Q L_{hole}}{L^2 \mathscr{D}} \quad (3)$$

With both systems provided the same flow rate, the ratio of Peclet numbers provides a measure for comparing the diffusive

(28) Goodrich, J. A., Kugel, J. F. *Binding and kinetics for molecular biologists;* Cold Spring Harbor Laboratory Press: Cold Spring Harbor, NY, 2007.
(29) Chaiken, I.; Rose, S.; Karlsson, R. *Anal. Biochem.* **1992**, *201*, 197–210.
(30) Myszka, D. G.; He, X.; Dembo, M.; Morton, T. A.; Goldstein, B. *Biophys. J.* **1998**, *75*, 583–594.
(31) Gervais, T.; Jensen, K. F. *Chem. Eng. Sci.* **2006**, *61*, 1102–1121.
(32) Yang, J.-C.; Ji, J.; Hogle, J. M.; Larson, D. N. *Nano Lett.* **2008**, *8*, 2718–2724.
(33) Gordon, R.; Brolo, A. G.; Sinton, D.; Kavanagh, K. L. *Laser Photonics Reviews* **2010**, *4*, 311–335.
(34) Im, H.; Lesuffleur, A.; Lindquist, N. C.; Oh, S.-H. *Anal. Chem.* **2009**, *81*, 2854–2859.
(35) Yue, S. L., Gu, C. Z. *7th IEEE Conference on Nanotechnology*; 2007; Vol. 1−3, pp 632−635.

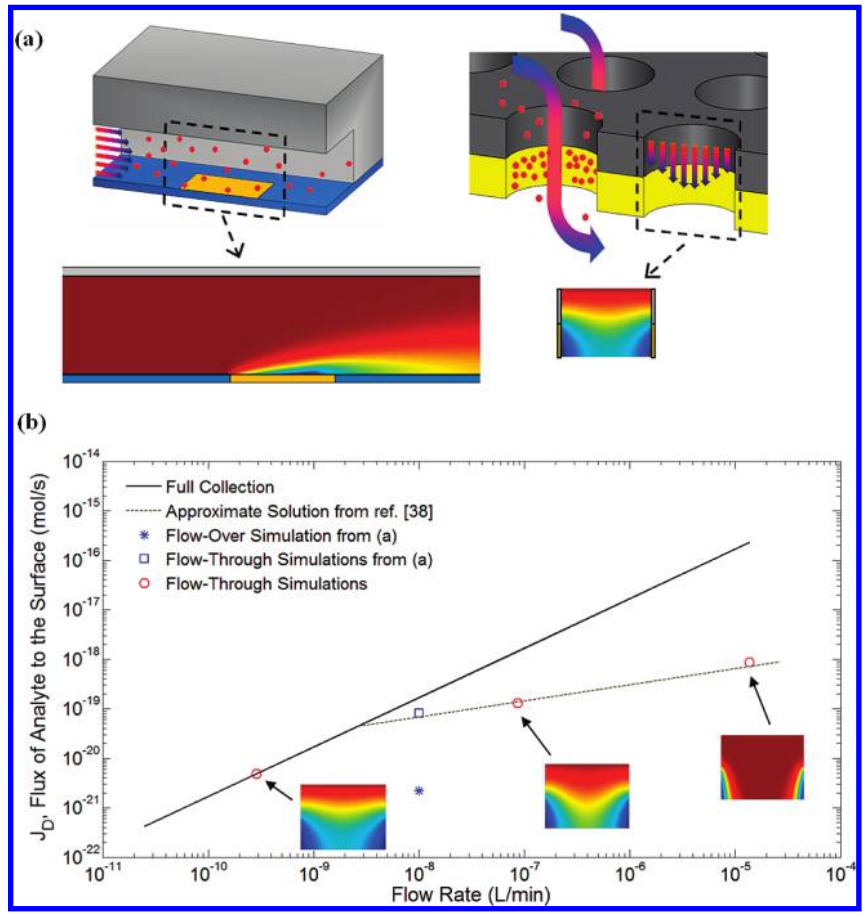

Figure 2. Comparison of transport in flow-over and flow-through sensing formats. (a) Schematic of the flow-over format (left) and flow-through format (right). Simulation results indicate analyte collection in the flow-over sensor ($L = H = 20\ \mu$m), and a flow-through nanohole ($D = 300$ nm, $L_{hole} = 100$ nm) array of equivalent sensing area. Both are provided the same flow rate ($Q = 10$ nL/min), $\mathscr{D} = 1 \times 10^{-10}$m^{2}s^{-1} and the surface concentration was fixed ($c_S(t) = 0$) to consider transport in isolation from binding kinetics. (b) Extension of results shown in (a) plotted as total molecular flux to the sensing surface, J_D, versus flow rate. The continuous line indicates the fundamental limit where all incoming analyte molecules are transported to the sensing surface. The dashed line represents the flux estimated using the solution for mass transfer to a two-dimensional sensor as given by Ackerberg et al.[38] Values corresponding to microchannel and nanohole cases from (a) are plotted, as indicated as in the legend, and sample flow-through flow-through computational results are shown inset.

transport of molecules to the sensing surface in each case as follows,

$$\frac{Pe_{ch}}{Pe_{hole}} = \frac{QL^2\mathscr{D}}{4QL_{hole}L\mathscr{D}} = \frac{L}{4L_{hole}} \tag{4}$$

Flow-over sensors in commercial systems have lengths on the order of $L \sim 40\ \mu$m,[30,36,37] while the depth of flow-through nanoholes, $L_{hole} \sim 100$ nm, is fixed by optical and fabrication considerations. Inputing these geometrical constraints in eq 4 provides a Peclet number ratio of 10^2. In other words, given the same flow rate and sensing area, the Peclet number inside the nanoholes is 2 orders of magnitude less than that in the channel with a typical flow-over sensor operating under otherwise similar conditions. The above scaling analysis suggests that flow-through nanohole array based sensing can provide up to 2 orders of magnitude more diffusive flux of analyte to the sensing surface as compared to a flow-over sensor, given the same sensing area and flow rate. This potential is further quantified in the computational transport analysis below.

Computational Transport Analysis. In order to provide a more detailed analysis of the transport in both sensing platforms, a computational model is employed. As in the scaling analysis above, binding kinetics in this section are assumed to be perfect and the surface concentration is set to $c_S(t) = 0$. This simplification allows the transport characteristics of the two sensing formats to be compared in isolation from surface binding kinetics (finite surface reaction rates and surface saturation are introduced in following section). The flow-over sensor is a square planar surface with $L = 20\ \mu$m. The flow-through sensor is an array of nanoholes with $D = 300$ nm, a gold thickness of $L_{hole} = 100$ nm and 10^3 nanoholes for equivalent sensing area to the flow-over case.

Figure 2a shows the results of the steady state simulations with perfect reaction kinetics for the case where $Q = 10$ nL/min of 1nM solution (with analyte diffusivity, $\mathscr{D} = 1 \times 10^{-10}$m^{2}s^{-1}) was provided to both systems. In the flow-over case, the depletion region is thin compared to the channel width and as a result the majority of target molecules are swept downstream before they can diffuse to the sensing area. In the nanohole flow-through case, the depletion zone extends across the entire

(36) Schuck, P.; Millar, D. B.; Kortt, A. A. *Anal. Biochem.* **1998**, *265*, 79–91.

Table 1. Diffusion Coefficient, Adsorption Constant, Desorption Constant, Affinity Constant Characteristic Binding Time Scale and Surface Concentration at Equilibrium for Analyte Systems 1−4

	analyte system 1	analyte system 2	analyte system 3	analyte system 4
$\mathscr{D}(m^2s^{-1})$	1×10^{-11}	1×10^{-10}	1×10^{-9}	1×10^{-9}
$k_{on}(s^{-1}M^{-1})$	1×10^{4}	2×10^{6}	1×10^{3}	1×10^{2}
$k_{off}(s^{-1})$	1×10^{-4}	2×10^{-3}	1×10^{-8}	1×10^{-7}
$K_A(M^{-1})$	1×10^{8}	1×10^{9}	1×10^{11}	1×10^{9}
τ (s)	1×10^{2}	4×10^{-1}	1×10^{3}	1×10^{4}
$c_S^{Eq}(mol \cdot m^{-2})$	1×10^{-6}	1×10^{8}	1×10^{8}	1×10^{8}

nanohole cross-section as the majority of analytes are transported to the inner-wall sensing surface.

Figure 2b quantifies analyte flux to the surface as function of total flow rate. Due to the mixture of length scales involved, both the flux of analyte to the sensor surface and the flow rate are given in dimensional forms, mol/s and L/min, respectively. The continuous line indicates the limit where all analytes entering the sensing platform (i.e., J_0) are transported to the sensing surface. The dashed line is the flux as estimated using the asymptotic solution for mass transfer for a two-dimensional sensor provided by Ackerberg et al.[38] Several aspects of Figure 2 are noteworthy: (1) As flow rate increases, total flux to the sensing surface increases in accordance with expected results;[38] (2) At low flow rates such as the point shown at $Q = 0.3$ nL/min, essentially all incoming analyte is transported to the sensing surface ($J_D/J_0 > 99\%$); (3) For the specific flow-through/flow-over comparison cases (shown in Figure 1a), the flow-through sensing format provides 40-fold more flux of analyte to the sensing surface (given same flow rate and sensing area).

Computational Transport and Binding Analysis. Finite binding kinetics, in general, have the effect of slowing down sensor response as compared to the idealized cases discussed above. In this context, it is informative to determine the kinetic conditions under which the flow-through nanohole array strategy is beneficial, and the conditions under which it provides negligible benefit. Toward this end, binding kinetics was included in the model for both the flow-over and flow-through cases. In order to characterize the kinetic binding systems in a way that is as general and widely applicable as possible, the characteristic binding time scale τ from eq 2 is employed.

The response times of the flow-over and flow-through sensing formats for four different analyte systems with binding kinetics and surface concentration saturation at equilibrium are summarized in Table 1. Analyte System 1 represents the binding of a relatively large, slow molecule with favorable binding kinetics, such as bovine serum albumin[39] (BSA). Analyte System 2 is an antibody−antigen system modeled after the common cancer biomarker CA125.[40] Analyte Systems 3 and 4 represent a generic small molecule bioassay with "on" kinetics that are fast and slow, respectively. Diffusion of the analyte to the surface will play a major role in cases 1 and 2, but the adsorption kinetics will be more important in cases 3 and 4. The binding kinetic time

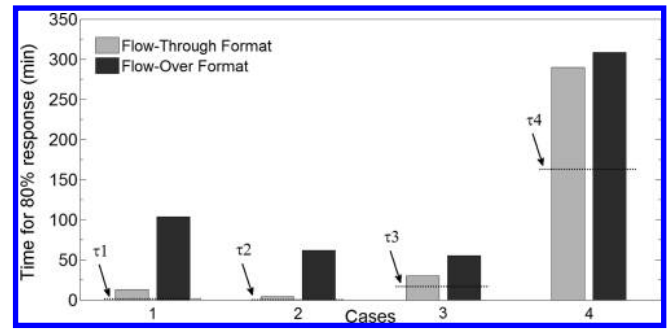

Figure 3. Comparison of flow-over and flow-through sensing formats for four analyte systems. Time for 80% of the equilibrium analyte concentration to be adsorbed to the surface is plotted for both sensing formats. The sensors had equivalent sensing area with geometries as employed in Figure 2, and both systems were provided 10 nL/min. The flow-through format provides significant gains for Analyte Systems 1 and 2, however, only a modest benefit was achieved in Systems 3 and 4. Particularly in Analyte System 4, the benefit of flow-through transport is obscured by the long characteristic time binding time. Characteristic binding time scale for each case is shown as a dashed line as indicated.

constant, τ, is calculated for each system in Table 1, and this value represents a minimum time scale (or maximum rate) for sensor response based on perfect transport. In this sense, τ imposes a speed limit that can be attained, but not exceeded, with improved transport schemes.

Figure 3 shows the response from each analyte system when implemented in flow-over and flow-through sensing formats. The sensors had equivalent sensing area with geometries as applied in Figure 2, and both systems were provided 10 nL/min and $c_0 = 10^{-9}$M. The response time was taken as the time for the sensor to have 80% of the equilibrium analyte concentration adsorbed to the surface. For system 1, the flow-through nanohole response time was approximately equivalent to the binding time scale, τ, indicating that the flow-through system approximates the perfect transport limit. For the flow-over case the sensor response was approximately eight times slower. The flow-through strategy also provided much faster response when applied to the Analyte System 2 (CA125 cancer biomarker). For Analyte System 3, however, the benefit of the flow-through nanohole approach was less significant. This was due to a combination of the smaller molecular size (increasing the diffusive transport rate in both systems) and the much slower (i.e., rate limiting) binding kinetics as indicated by the large characteristic τ value. Analyte System 4 represents a further extreme, where binding kinetics limit the process entirely. Although the flow-through strategy provided a faster response, the time savings are not significant as compared to the long characteristic binding time ($\tau = 10^3$s.) These cases illustrate a spectrum of sensor responses for four analyte systems, and while the flow-through format provides significant gains for Analyte System 1 and 2, only a modest benefit was achieved in Systems 3 and 4.

Figure 4 provides sensor time response as a function of the characteristic binding time scale, τ, spanning 5 orders of magnitude. In these simulations, the adsorption constant was varied as $10^2 \leq k_{on} \geq 10^7$ $M^{-1}s^{-1}$, keeping constant values of k_{off}, $c_0 = 10^{-6}$ M and $Q = 2$ μL/min. The desorption kinetic constant, k_{off}, was fixed at a constant and sufficiently low value (10^{-5} s^{-1}) to

(37) Natarajan, S.; Katsamba, P. S.; Miles, A.; Eckman, J.; Papalia, G. A.; Rich, R. L.; Gale, B. K.; Myszka, D. G. *Anal. Biochem.* **2008**, *373*, 141–146.
(38) Ackerberg, R. C.; Patel, R. D.; Gupta, S. K. *J. Fluid Mech.* **1978**, *86*, 49–65.
(39) Meechai, N.; Jamieson, A. M.; Blackwell, J. *J. Colloid Interface Sci.* **1999**, *218*, 167–175.
(40) Xie, C.; Dong, C.; Ren, J. *Talanta* **2009**, *79*, 971–974.

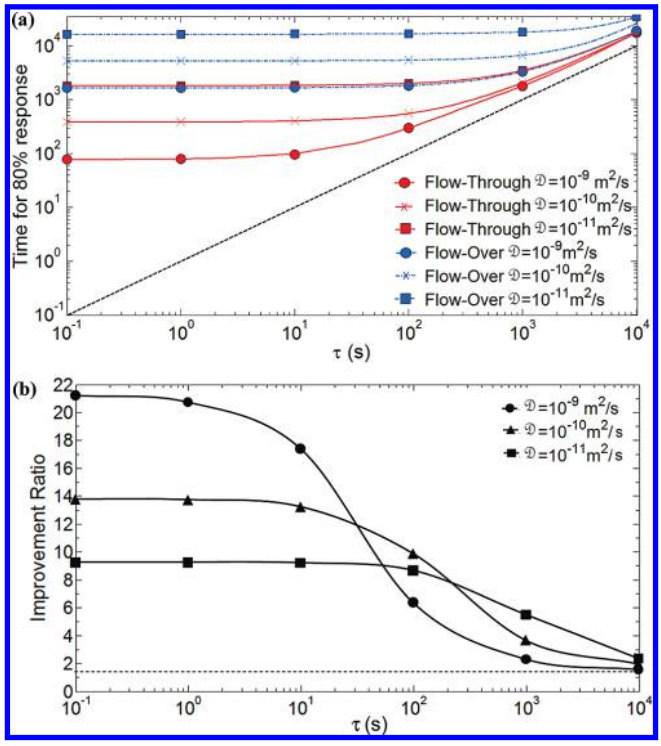

Figure 4. Response time improvement of the flow-through sensing format as a function of characteristic binding time scale, τ. The results shown in (a) were obtained from simulations using the COMSOL model described in the text, and varying k_{on} from 10^2 to 10^7 $M^{-1}s^{-1}$ for three different molecule sizes. In all cases, c_0 is higher than $1/K_A$ to ensure saturation of the sensing surface. The flow-through format provides maximum benefit at $\tau \leq 10^2$ s. As τ increases, all the response curves approach the limit $t = \tau$. In (b), the results from (a) are shown as a flow-through-to-flow-over response time improvement factor. The highest benefit, around 20-fold, is achieved for rapidly diffusing analyte and smaller τ values; and between 10- to 20-fold for values representing typical biosensing applications.[40,42,43]

ensure the process was dictated by the "on" kinetics (this is representative of many bioassays, having k_{on} values in the range of 10^3 to 10^5 $M^{-1}s^{-1}$ and k_{off} values $\sim 10^{-5}$).[39−41] In order to include the effect of the analyte size, the simulations were performed considering three different analyte diffusivities, 10^{-11}, 10^{-10}, and 10^{-9} m^2/s, spanning the range of cases in Table 1. As shown in Figure 4a, the flow-through nanohole system provides maximum benefit at low τ values corresponding to fast reaction kinetics. As τ increases, binding kinetics become dominant and all response curves asymptotically approach the limit $t = \tau$.

Figure 4b provides a measure of the improvement achieved by employing the flow-through format. Specifically, the results are plotted in terms of an improvement factor, defined as the ratio of flow-over format to flow-through format response times. As shown, a benefit of 20-fold was achieved for small (rapidly diffusing) analytes with relatively fast binding kinetics ($\tau < 1$ s). As the binding time scale increases, the benefit decreases. These results indicate that a significant benefit (i.e., 2-fold improvement in response time) is achieved even for cases with binding time constants up to $10^3 s$. Many biosensor applications employ analytes with binding time constants in the range of $1-10^2$ s.[17,39,42,43] In that range, flow-through nanohole array sensors can provide ~10- to 20-fold improvement in response. It is interesting to note that although the highest improvement ratios are achieved with small analytes (high diffusivity) with fast reaction kinetics, the benefits are eroded rapidly as the binding kinetics slow down. In contrast, larger analytes (low diffusivity) maintain significant benefits with slower binding kinetics, for example, $\mathscr{D} = 10^{-11} m^2/s$ maintains 5-fold improvement up to $\tau = 10^3$ s.

CONCLUSIONS

In this work, the analyte transport and time response of flow-through nanohole arrays was quantified and compared with that of a traditional flow-over sensor in a microchannel. The transport scaling analysis indicated that the flow-through sensor exhibits a Peclet number, Pe, 10^2-fold less than the flow-over format for the same given flow rate. For the case of rapid surface kinetics, the computational results indicated that, the flux of analyte molecules to the sensing surface of a flow-through nanohole array was much higher than the flow-over sensor (40-fold higher in the case of $Q = 10$ nL/min).

Finite binding kinetics, in general, have the effect of slowing down sensor response as compared to the purely transport limited case. Binding kinetics were included in the model, and the system response times were compared as a function of binding time constant and diffusion coefficient. A 20-fold faster time response, was achieved for the flow-through case with small (rapidly diffusing) analytes with relatively fast reaction kinetics. In the range applicable to most biosensing applications ($\tau = 1 - 10^3 s$), and analytes with typical diffusion coefficients ($\mathscr{D} = 10^{-11}$ to 10^{-9} m^2/s), flow-through nanohole arrays offer ~10-fold benefit in terms of time response over established flow-over sensors formats.

ACKNOWLEDGMENT

We gratefully acknowledge the financial support of the Natural Sciences and Engineering Research Council of Canada, NSERC, through a scholarship to CE and research grant in partnership with the BC Cancer Agency Trev and Joyce Deeley Antibody Research Unit and Micralyne Inc. Funding from the Canada Research Chairs Program, the Canada Foundation for Innovation, and the British Columbia Knowledge Development Fund are also gratefully acknowledged.

SUPPORTING INFORMATION AVAILABLE

Additional information and figures. This material is available free of charge via the Internet at http://pubs.acs.org.

Received for review June 23, 2010. Accepted November 2, 2010.

AC101654F

(41) Sahu, A.; Soulika, A. M.; Morikis, D.; Spruce, L.; Moore, W. T.; Lambris, J. D. *J. Immunol.* **2000**, *165*, 2491–2499.

(42) Laffly, E.; Pelat, T.; Cédrone, F.; Blésa, S.; Bedouelle, H.; Thullier, P. *J. Mol. Biol.* **2008**, *378*, 1094–1103.

(43) Zhang, X. Y.; Young, M. A.; Lyandres, O.; Van Duyne, R. P. *J. Am. Chem. Soc.* **2005**, *127*, 4484–4489.